Computing the thermal transport coefficient of neutral amorphous polymers using exact vibrational density of states: Comparison with experiments

Debashish Mukherji *

Quantum Matter Institute, University of British Columbia, Vancouver, Canada V6T 1Z4

(Received 29 May 2024; revised 11 July 2024; accepted 26 July 2024; published 8 August 2024)

Thermal transport coefficient κ is an important property that often dictates broad applications of a polymeric material, while at the same time its computation remains challenging. In particular, classical simulations overestimate the measurements of κ in comparison to those of the experiments and thus hinder their meaningful comparison. This is even when very careful simulations are performed using the most accurate empirical potentials. A key reason for such a discrepancy is because polymers have quantum-mechanical, nuclear degrees of freedom whose contribution to the heat balance is nontrivial. In this work, two semianalytical approaches are considered to accurately compute κ by using the exact vibrational density of states $g(\nu)$. The first approach is based within the framework of the minimum thermal conductivity model, while the second uses computed quantum heat capacity to scale κ. The computed κ of a set of commodity polymers compares quantitatively with κ^{expt}.

DOI: 10.1103/PhysRevMaterials.8.085601

I. INTRODUCTION

Thermal transport coefficient κ measures the ability of a material to conduct the heat current [1–5]. Here, κ is directly related to the heat capacity c, the group velocity v_g, and the phonon mean free path $\Lambda = \tau v_i$, with τ being the phonon lifetime [6]. Traditionally, extensive efforts have been devoted to investigating κ behavior in the crystalline materials [2,7–9]. The recent interest is more devoted to the polymeric solids [3,4,10–13]. This is particularly because polymers are an important class of soft matter, where the relevant energy scale is of the order of $k_B T$ at a temperature $T = 300$ K and k_B being the Boltzmann constant, and thus their properties are dictated by large conformational and compositional fluctuations [14–17]. This soft nature of polymers makes them important in designing flexible advanced materials with tunable thermal properties.

Polymers are a special case, where there are two main microscopic interactions, i.e., the intramolecular interactions along a chain contour and the nonbonded interactions between the neighboring monomers. In this context, κ of amorphous polymers is dictated by the localized vibrations that are usually only within the range of direct nonbonded contacts (i.e., Λ is very small) and thus are dominated by the monomer-monomer interactions [18,19], which in the nonconducting polymers can either be van der Waals (vdW) or hydrogen bonded (H bond) [17,20]. Because of the above reasons, polymers fall in the low κ materials [3,4], having typical values that are several orders of magnitude smaller than the standard crystals [1,2]. For example, the experimentally measured $\kappa^{\text{expt}} \simeq 0.1$–$0.2$ W/Km in vdW polymers [11,21], while $\kappa^{\text{expt}} \to 0.4$ W/Km in the H-bonded systems [10,11].

Extensive experimental and simulation efforts have been devoted to establish a structure-property relationship in polymeric solids with a goal to obtain a tunable κ. Here, the standard classical simulation techniques are of particular importance. However, routinely employed classical setups often overestimate κ^{cl} in comparison to κ^{expt} [22–24] and thus hinders their meaningful comparison. Complexities get even more elevated when dealing with systems at different thermodynamic state points [25,26], complex macromolecular architectures [27,28], and/or relative compositions in the case of multicomponent mixtures [10,11,29].

One can simply argue that $\kappa^{\text{cl}} > \kappa^{\text{expt}}$ might be due to the inaccuracies in classical force-field parameters and in the κ^{cl} calculations. While simulation errors are certainly inevitable, it may still be presumptuous to come to such a trivial conclusion because of the complexities of underlying macromolecular systems. A closer look at an amorphous polymer reveals that the nonbonded interactions are soft that dictate polymer properties (i.e., low ν anharmonic classical modes), while the intramolecular interactions along a chain backbone are stiff [23,30,31]. For example, the vibrational frequency of a C-H bond in polymers is $\nu \simeq 90$ THz [23,30]. Note that C-H is a common building block of most commodity polymers. Such a stiff mode and many other modes in a polymer remain quantum mechanically frozen at $T = 300$ K (with a representative frequency $\nu_{\text{room}} \simeq 6.2$ THz). On the contrary, however, a classical setup by default considers all modes (irrespective of their nature), and thus overestimates c [23,32] or κ [21,23,24] in polymers.

The discussions above pose a grand challenge on how to accurately compute κ in polymeric solids with a goal to achieve their meaningful (quantitative) comparison with κ^{expt}. Motivated by this need, the present work uses two simple semianalytical approaches using the exact vibrational density of states $g(\nu)$ to estimate κ at different thermodynamic state

*Contact author: debashish.mukherji@ubc.ca

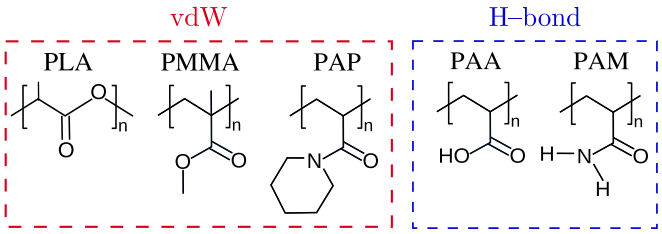

FIG. 1. Schematics representation of the commodity polymeric structures investigated in this study. The red panel compiles the van der Waals (vdW) based systems, i.e., poly(lactic acid) (PLA), poly(methyl methacrylate) (PMMA), and poly(*N*-acryloyl piperidine) (PAP). The blue panel shows two examples of hydrogen bonded (H bond) polymers, i.e., poly(acrylic acid) (PAA) and polyacrylamide (PAM).

points. While the first approach (Approach I) is based within the well-known framework of the minimum thermal conductivity model (MTCM) [33], another approach (Approach II) estimates κ by the accurate computation of quantum c [23]. To validate our scenarios, this work investigates a set of experimentally relevant amorphous (commodity) polymers (see Fig. 1).

The remainder of the paper is organized as follows: In Sec. II the system specific details and the corresponding force field parameters are highlighted. The results are discussed in Sec. III and finally the conclusions are drawn in Sec. IV.

II. MATERIALS, MODEL, AND METHOD

In this work, a set of five commodity polymers, covering across vdW and H-bonded systems, namely, poly(lactic acid) (PLA), poly(methyl methacrylate) (PMMA), poly(*N*-acryloylpiperidine) (PAP), polyacrylamide (PAM), and poly(acrylic acid) (PAA) are investigated. The monomer structures of these systems are shown in Fig. 1. The specific systems are chosen because their detailed experimental data are available [11,19,25,34] and also because of their available well-equilibrated configurations for all these samples [21,23]. In particular, the computed κ are compared with κ^{expt} at one thermodynamics state point for PMMA, PAP, PAM, and PAA, while the T-dependent $\kappa(T)$ are only shown for PMMA and PLA. The latter is because, to the best of our knowledge, the experimental data for $\kappa(T)$ is not available for PAA and PAM.

The chain length $N_\ell = 30$ is taken for all systems, except for PAM where $N_\ell = 32$. Each system consists of 200 chains within a cubic simulation box. The standard OPLS–AA force-field parameters [35] are used for PLA, PAP, and PAA, while a set of modified parameters are used for PMMA [36] and PAM [37]. Simulations are performed using the GROMACS package [38].

Temperature is imposed using the velocity-rescaling thermostat [39] with a damping time of $\tau_T = 1$ ps, and the pressure is set to 1 atm with a Berendsen barostat [40] with a time constant $\tau_p = 0.5$ ps. Electrostatics are treated using the particle-mesh Ewald method. The interaction cutoff for the nonbonded interactions are chosen as $r_c = 1.0$ nm. The simulation time step is set to $\Delta t = 1$ fs during equilibration and the equations of motion are integrated using the leapfrog algorithm.

All these polymers were equilibrated earlier in their (solvent-free) melt states at $T = 600$ K for at least 1 μs each sample, i.e., 500 ns in Ref. [21] and another 500 ns in Ref. [23]. Note that $T = 600$ K is at least 150 K above their calculated glass transition temperatures [21]. For this study, these melt equilibrated samples were individually quenched to $T = 300$ K with a rate 0.04 K/ns for a total of 7.5 μs per sample. The total simulation time accumulated for this study alone is over 40 μs.

III. RESULTS AND DISCUSSIONS

A. Vibrational density of states

A key observable for this study is $g(\nu)$. For this purpose, the mass-weighted velocity autocorrelation function is calculated using

$$c_{\text{vv}}(t) = \sum_i m_i \langle \overrightarrow{v}_i(t) \cdot \overrightarrow{v}_i(0) \rangle. \tag{1}$$

Here, m_i and $\overrightarrow{v}_i$ are the mass and the velocity of ith particle, respectively. $c_{\text{vv}}(t)$ is calculated under the microcanonical ensemble with $\Delta t = 0.1$ fs and the data is sampled for 10 ps with an output data frequency of 5×10^{-4} ps. A representative $c_{\text{vv}}(t)/c_{\text{vv}}(0)$ for PLA is shown in Fig. 2(a). The long-lived fluctuations are clearly visible in the global $c_{\text{vv}}(t)$ that originates from the superposition of normal modes and thus its Fourier transform results in $g(\nu)$ [23,41] using

$$g(\nu) = \frac{1}{C} \int_0^\infty \cos(2\pi\nu t) \frac{c_{\text{vv}}(t)}{c_{\text{vv}}(0)} \mathrm{d}t, \tag{2}$$

where the prefactor C ensures $\int g(\nu)\mathrm{d}\nu = 1$. Figures 2(b) and 3 show $g(\nu)$ for a PLA, and another set of four commodity polymer samples, respectively. It can be appreciated that there are many high ν modes in these systems, i.e., for $\nu > \nu_{\text{room}} \simeq 6.2$ THz, that contribute rather nontrivially at a given T.

Given the discussions above, if the contributions of different modes are not properly accounted within a calculation, it will automatically lead to a wrong estimate of κ. Therefore, in the next sections, $g(\nu)$ shown in Figs. 2 and 3 will be used to accurately compute κ.

B. Approach I: Computation of κ using $g(\nu)$

The first approach is based within the framework of the well-known minimum thermal conductivity model (MTCM) [33]. To this end, the general expression of κ for a three-dimensional isotropic material reads [6]

$$\kappa(T) = \left(\frac{\rho_{\text{N}} h^2}{3k_{\text{B}}T^2}\right) \sum_i \int \tau(\nu) v_{g,i}^2(\nu) \frac{\nu^2 e^{h\nu/k_{\text{B}}T}}{\left(e^{h\nu/k_{\text{B}}T} - 1\right)^2} g(\nu)\mathrm{d}\nu, \tag{3}$$

where $\rho_{\text{N}} = N/V(T)$ is the total atomic number density, N the total number of atoms, and h the Planck constant. Starting with Eq. (3) and for the nonconducting amorphous solids, MTCM proposed that Λ is limited to half the phonon wavelength and thus approximates $\tau(\nu) = 1/2\nu$ [6,33]. Also, $v_g \simeq v_i$ with v_i being the components of sound wave velocity. This

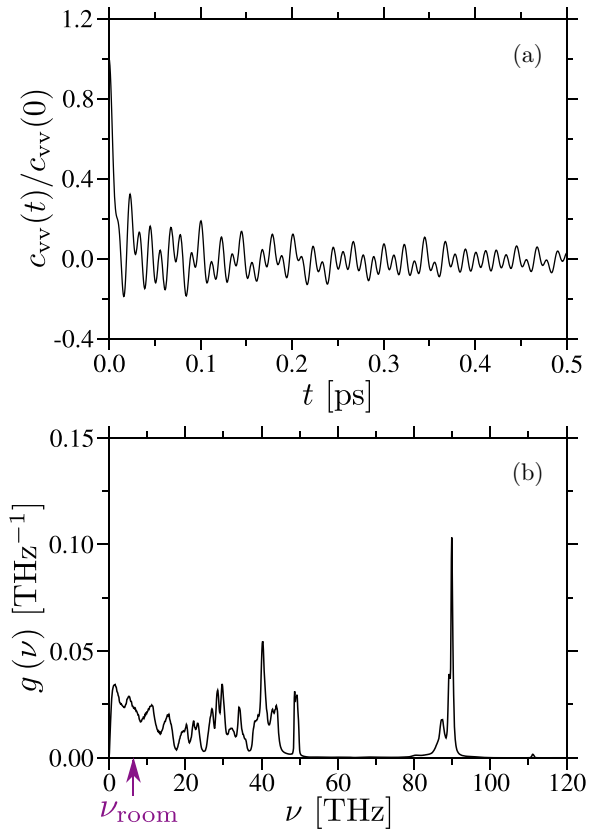

FIG. 2. Part (a) shows a normalized mass-weighted velocity autocorrelation function $c_{vv}(t)/c_{vv}(0)$ for poly(lactic acid) (PLA) at a temperature $T = 300$ K. The vibrational density of states $g(\nu)$ of PLA is shown in part (b), where $g(\nu)$ is calculated using Eq. (2). The arrow in part (b) indicates the vibrational frequency $\nu_{room} \simeq 6.2$ THz corresponding to $T = 300$ K.

description gives

$$\kappa = \left(\frac{\rho_N h^2}{6k_B T^2}\right)\left(v_\ell^2 + 2v_t^2\right)\mathcal{I}(T) \tag{4}$$

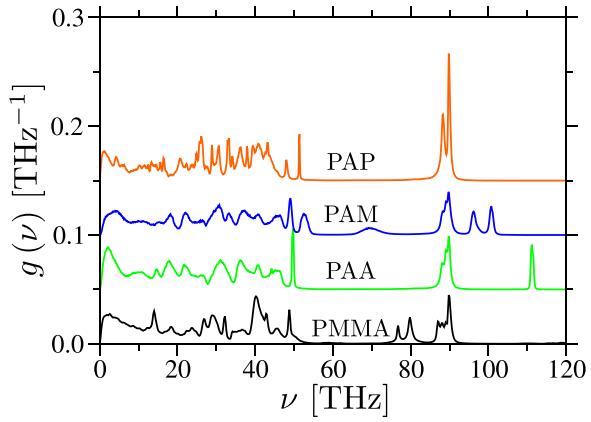

FIG. 3. Same as Fig. 2(b); however, for four other commodity polymers, namely, poly(*N*-acryloyl piperidine) (PAP), polyacrylamide (PAM), poly(acrylic acid) (PAA), and poly(methyl methacrylate) (PMMA). Individual $g(\nu)$ are shifted for a clearer representation.

and

$$\mathcal{I}(T) = \int \frac{\nu e^{h\nu/k_B T}}{\left(e^{h\nu/k_B T} - 1\right)^2} g(\nu)\mathrm{d}\nu. \tag{5}$$

$v_\ell = \sqrt{C_{11}/\rho_m}$ and $v_t = \sqrt{C_{44}/\rho_m}$ are the longitudinal and the transverse sound wave velocities, respectively. Here, $C_{11} = K + 4C_{44}/3$, K is the bulk modulus, C_{44} is the shear modulus, and ρ_m is the mass density. It can be appreciated in Eq. (4) that κ is directly related to the materials stiffness via v_ℓ and v_t.

Standard theoretical approaches typically use the Debye form of the parabolic density of states $g_D(\nu) = 3\nu^2/\nu_D^3$ in Eq. (4), where ν_D is the Debye frequency [6,41],

$$\nu_D = \left(\frac{9\rho_N}{4\pi}\right)^{1/3}\left(\frac{1}{v_\ell^3} + \frac{2}{v_t^3}\right)^{-1/3}. \tag{6}$$

The Debye temperature $\Theta_D = h\nu_D/k_B$. In Table I, ν_D and Θ_D values are listed for four different polymers. Note that these values are calculated using the experimental data of v_ℓ and v_t taken from Ref. [11], while ρ_N are from our simulations. It can be seen that Θ_D (or ν_D) are about 20%–40% lower than $T = 300$ K (or $\nu_{room} = 6.2$ THz), which is expected because of the dominant nonbonded interactions. Something that speaks in this favor is that Θ_D for the weak vdW systems (PAP and PMMA) are about 40–50 K lower than the polymers dictated by the relatively stronger H bonds (PAA and PAM).

The choice of $g_D(\nu)$ is certainly a good approximation for the standard (nonpolymeric) solids where typically $\Theta_D \gg T = 300$ K. However, $g_D(\nu)$ in polymers [having rather complex $g(\nu)$, as in Figs. 2(b) and 3] often tend to overestimate the contributions from the low-frequency vibrational modes. Something that supports this claim is that MTCM using $g_D(\nu)$ predicts values comparable to κ^{expt} in nonpolymeric amorphous solids [33]. However, for the polymers under the high-temperature conditions, MTCM systematically estimates higher values than κ^{expt} [11].

This study revisits MTCM using the exact $g(\nu)$ from Fig. 3 in Eq. (4). Computed κ for four different systems are listed in Table I. It can be appreciated that κ matches within 1%–25% of κ^{expt}. An illustrative plot comparing κ values between different approaches are compiled in Fig. 4.

It should also be noted that the stiffness of a polymeric material is dictated by the nonbonded interactions that are classical in nature. Therefore, carefully conducted classical polymer simulations can give reasonable estimates of the elastic moduli comparable to the corresponding experimental values. On the contrary, however, quantum effects are important in the crystalline solids, i.e., for $T \ll \Theta_D$ [42,43]. It might also be important to highlight that the $\tau(\nu) \propto 1/\nu$ behavior is valid for the amorphous systems under the high-temperature conditions, while one may expect $\tau(\nu) \propto 1/\nu^2$ for the crystalline solids strictly when the harmonic approximation holds [44].

C. Approach II: Scaling κ using quantum estimate of heat capacity

The results in Sec. III B are presented at one thermodynamic state point, i.e., at $T = 300$ K. This is specifically because, to the best of our knowledge, the data for v_ℓ and v_t are not available over a range of T for the

TABLE I. Longitudinal v_ℓ and transverse v_t sound velocities, the Debye frequency ν_D, the Debye temperature Θ_D, and the experimental thermal transport coefficient κ^{expt}. The thermal transport coefficient κ calculated using Eq. (4) is listed together with its variation with respect to κ^{expt}. The experimental values of v_ℓ, v_t, and κ^{expt} are taken from Ref. [11], while the total atom number density ρ_N and vibrational density of states $g(\nu)$ are computed from simulations. The data is shown for a temperature $T = 300$ K and for four different polymers, namely, poly(methyl methacrylate) (PMMA), poly(acrylic acid) (PAA), polyacrylamide (PAM), and poly(*N*-acryloyl piperidine) (PAP).

Polymer	v_ℓ^{expt} (nm/ps)	v_t^{expt} (nm/ps)	ν_D (THz)	Θ_D (K)	κ^{expt} (W m^{-1} K^{-1})	κ (W m^{-1} K^{-1})	$\frac{\lvert\kappa^{expt}-\kappa\rvert}{\kappa^{expt}}$ (%)
PMMA	2.85	1.30	3.75	180.27	0.20	0.21	5.0
PAA	3.74	1.72	4.60	220.93	0.37	0.41	10.8
PAM	4.34	1.82	4.88	234.17	0.38	0.32	15.8
PAP	2.64	1.30	3.80	182.58	0.16	0.20	25.0

polymers listed in Table I. Therefore, in this section, a slightly different (yet related) framework is used to compute T-dependent $\kappa(T)$. For this purpose, the classical estimate of the thermal transport coefficient κ^{cl} is first calculated using the approach-to-equilibrium (ATE) method [45].

In ATE, a simulation box with a length L_x along the x direction is divided into three regions, i.e., the middle region of width $L_x/2$ is sandwiched between two side regions of equal width $L_x/4$. The middle slab is kept at an elevated temperature $T_{hot} = T + 50$ K, while the two side slabs are maintained at a lower temperature $T_{cold} = T - 50$ K. Here, T_{hot} and T_{cold} are the kinetic temperatures of the hot and the cold regions, respectively. T refers to a reference temperature at which $\kappa^{cl}(T)$ is calculated. In the first step, these regions are thermalized under the canonical simulations for 5 ns with $\Delta t = 1$ fs. After this stage, $\Delta T(t) = T_{hot} - T_{cold}$ is allowed to relax during a set of microcanonical runs for 50 ps with $\Delta t = 0.1$ fs. From an exponential relaxation of $\Delta T(t) \propto \exp(-t/\tau_x)$, the time constant τ_x for the energy flow along the x direction is

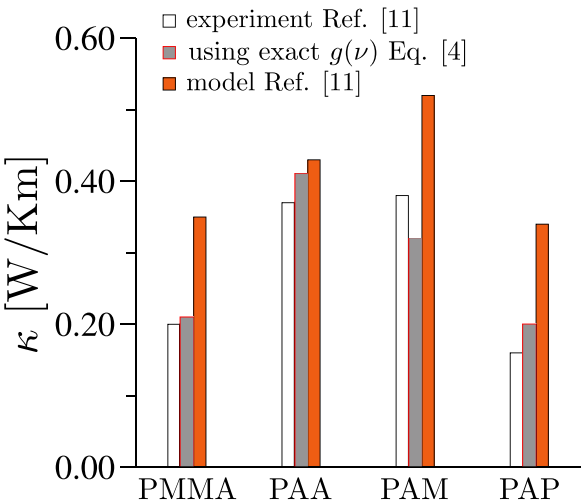

FIG. 4. A comparative plot of the thermal transport coefficient κ at a temperature $T = 300$ K. The data is shown for four different polymers, namely, poly(methyl methacrylate) (PMMA), poly(acrylic acid) (PAA), polyacrylamide (PAM), and poly(*N*-acryloyl piperidine) (PAP). The experimental data for these polymers are taken from Ref. [11], while the simulation data is calculated using the exact density of states $g(\nu)$ from Fig. 3 in Eq. (4). For comparison, the high T estimates from the minimum thermal conductivity [11] with corrections of the stiff modes are also included.

calculated. Finally, $\kappa^{cl}(T)$ can be estimated using [45]

$$\kappa^{cl}(T) = \frac{1}{4\pi^2}\frac{c^{cl}(T)L_x}{A\tau_x}. \tag{7}$$

A is the cross-section area of a sample. The classical estimate of specific heat is calculated using $c^{cl}(T) = H(T+\Delta T) - H(T-\Delta T)/2\Delta T$ and the enthalpy is $H(T) = U(T) + pV(T)$. $U(T)$ is the internal energy including the mean kinetic energy, $p = 1$ atm is the external pressure, and $V(T)$ is the system volume. The computed $\kappa^{cl}(T)$ for the PLA and PMMA samples are shown in Fig. 5 (see the • data sets). It is clearly visible that $\kappa^{cl}(T)$ is about a factor of 2 to 3 times larger than the corresponding $\kappa^{expt}(T)$.

Note that for $T > \Theta_D$ (as in the commodity polymers listed in Table I), τ_x is dominated by the nonbonded (classical) interactions [19]. On the contrary, the intramolecular stiff interactions along a chain contour do not contribute to τ_x, yet they are by default incorporated in $c^{cl}(T)$ and thus $\kappa^{cl}(T) > \kappa^{expt}(T)$. This is consistent with the data that the difference between $c^{cl}(T)$ and $c^{expt}(T)$ is also about a factor of 2 to 3 (see the • data sets and the lines in the Appendix, Fig. 6).

Within the above discussion, if one can use the accurate estimate of $c(T)$ in Eq. (7) by properly accounting for the contributions from the vibrational mode at a given T [23,46], one may just simply get the quantum corrected estimate of $\kappa(T)$. For this purpose, $c(T)$ is calculated using a recently proposed method [23]. In a nutshell, this method uses the Binder approach [41] to estimate the contributions of the stiff harmonic modes and thus their total contribution is given by

$$\frac{c_h(T)}{k_B} = \frac{h^2}{k_B^2T^2}\int_0^\infty \frac{\nu^2 e^{h\nu/k_BT}}{(e^{h\nu/k_BT}-1)^2}g(\nu)d\nu, \tag{8}$$

which is then used to get the difference $\Delta c(T)$ between the classical and the quantum descriptions,

$$\frac{\Delta c(T)}{k_B} = \int_0^\infty \left\{1 - \left(\frac{h\nu}{k_BT}\right)^2 \frac{e^{h\nu/k_BT}}{(e^{h\nu/k_BT}-1)^2}\right\} g(\nu)d\nu, \tag{9}$$

and finally gives the quantum corrected estimate [23],

$$c(T) = c^{cl}(T) - \Delta c(T). \tag{10}$$

The main advantage of this approach is that the contributions of the stiff harmonic modes are corrected, while the contributions from the soft (anharmonic) modes remain unaltered and thus do not alter the macroscopic polymer properties. In the Appendix, Fig. 6, quantum corrected $c(T)$ for PLA and PMMA samples are shown. As expected, the quantum

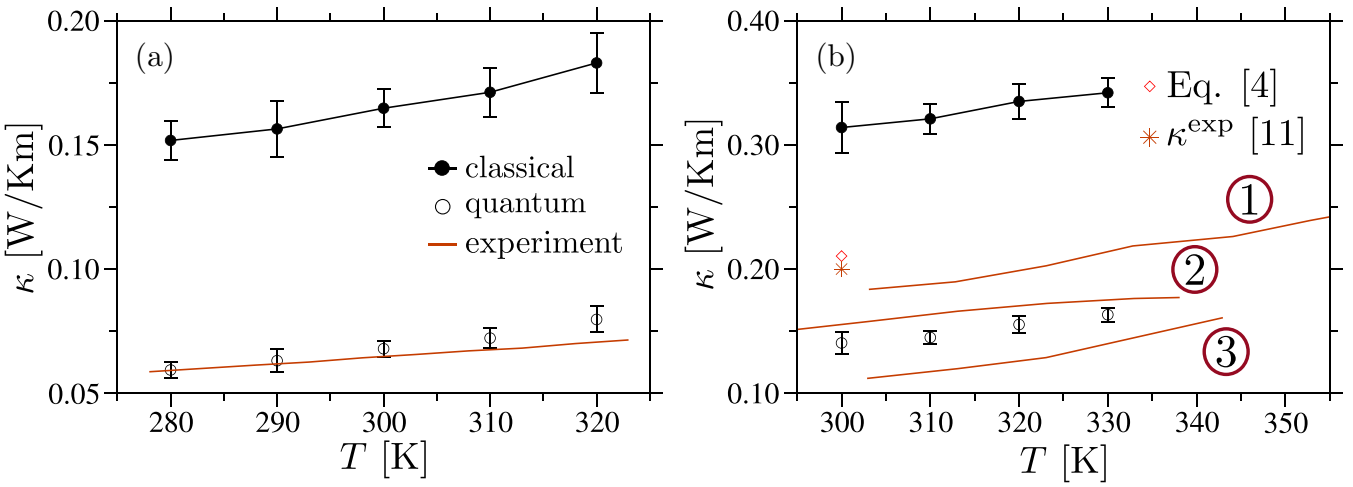

FIG. 5. Thermal transport coefficient κ as a function of temprature T for poly(lactic acid) (PLA) (a) and poly(methyl methacrylate) (PMMA) (b). For comparison experimental data are also included. The experimental data of PLA is taken from Ref. [25]. The PMMA experimental data sets 1–3 are taken from Refs. [19,26,34], respectively.

correction discussed above gives reasonable estimates of $c(T)$ in comparison to $c^{\text{expt}}(T)$. The calculated $c(T)$ is then used to obtain quantum corrected $\kappa(T)$ using

$$\kappa(T) = \frac{1}{4\pi^2}\frac{c(T)L_x}{A\tau_x}. \tag{11}$$

The resultant data is shown in Fig. 5 (see the ○ data sets). It can be appreciated that this simple approach in Eq. (11) gives reasonable estimates of $\kappa(T)$.

IV. CONCLUSIONS AND DISCUSSIONS

This work used a conventional classical molecular dynamics setup to estimate the quantum corrected thermal transport coefficient κ in polymeric solids. For this purpose, the exact vibrational density of states $g(\nu)$ is used as a key observable within two different (yet related) semianalytical approaches. In one approach, κ is computed within the framework of the minimum thermal conductivity model [33], while another approach simply uses the quantum estimate of specific heat $c(T)$ as a correction to $\kappa(T)$. The data for a set of five different commodity polymers show reasonable agreement with the experiments, at one thermodynamic state point and also with changing T. Therefore, this work attempts to highlight a couple of simple approaches to obtain quantum κ from classical simulations. The approaches presented herein can also be used in studying κ under the high-pressure conditions. One key application is in the field of hydrocarbon-based oils [23,24] under high pressures.

It is also important to highlight that the approaches discussed here are valid for the nonconducting amorphous polymers, where localized vibrations carry the heat current [19]. These vibrations are dictated by the nonbonded interactions between the neighboring monomers and are classical in nature. Therefore, by simply eliminating the contributions of the intramolecular stiff modes, reasonable estimates of $\kappa(T)$ can be calculated. However, when dealing with the chain-oriented systems [47], such as in the polymer fibers [47] or in the molecular forests [48], the situation is somewhat different. This is particularly because κ is an extended configuration that is dominated by the stiff intramolecular interactions, i.e., almost a representative of the crystalline

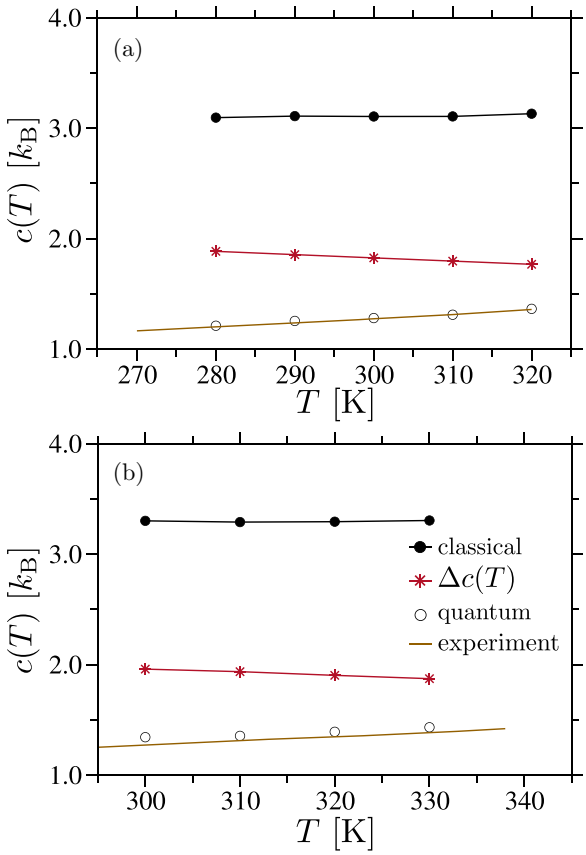

FIG. 6. Per particle specific heat $c(T)$ as a function of temperature T for poly(lactic acid) (PLA) (a) and poly(methyl methacrylate) (PMMA) (b). The data is shown for the classical estimate of specific heat $c^{\text{cl}}(T)$, correction factor $\Delta c(T)$ using Eq. (9), and quantum specific heat $c(T)$ using Eq. (10). For comparison experimental data are also included. The PLA and PMMA data is taken from Refs. [26,57], respectively.

structures along the chain backbone [49–51]. For example, a standard amorphous polymer usually has $\kappa \simeq 0.1$–0.4 W/Km [3,10,11,52], while the expanded chain configurations usually have $\kappa \geqslant 100$ W/Km [47,48]. Another set of systems where intramolecular interactions dictate κ is the highly cross-linked networks, where a delicate balance between the bond density, network microstructure, and bond property controls κ [27,28,53].

A simplistic scaling correction in Eq. (11) may not be appropriate for the crystalline solids with long-range order, where propagating phonons carry the heat current [6]. Here, it was readily observed that the representative hump in $\kappa^{\text{expt}}(T)$ for the crystals happen at a T that is far lower than the typical plateau in $c(T)$, i.e., the anharmonic effects already become relevant at $T \ll \Theta_{\text{D}}$. For example, in crystalline silicon, a hump in κ happens between 10–20 K [54], while $\Theta_{\text{D}} > 600$ K. In such systems, therefore, quantum effects must be properly incorporated via $\tau(\nu, T)$, $v_i(T)$, and also $c(T)$ in Eq. (4). In this context, there are detailed theoretical approaches that deal with the accurate calculation of κ in crystalline materials [55,56].

ACKNOWLEDGMENTS

The content presented in this work would not have been possible without numerous very stimulating discussions with Martin Müser during the preparation and after the publication of our collaborative work in Ref. [23], whom I take this opportunity to gratefully acknowledge. I also thank Robinson Cortes–Huerto and Vedangi Pathak for useful discussions. I further thank the Advanced Research Computing facility where simulations are performed. This research was undertaken thanks, in part, to the Canada First Research Excellence Fund (CFREF), Quantum Materials and Future Technologies Program.

APPENDIX: QUANTUM HEAT CAPACITY OF POLYMERS

Figure 6 shows the comparative data sets for heat capacity. While the classical estimate $c^{\text{cl}}(T)$ is overestimated, a simple quantum correction using Eq. (10) eliminates the unwanted contributions from the high ν stiff modes and thus gives a better comparison between $c(T)$ and $c^{\text{expt}}(T)$.

[1] D. G. Cahill, W. K. Ford, K. E. Goodson, G. D. Mahan, A. Majumdar, H. J. Maris, R. Merlin, and S. R. Phillpot, Nanoscale thermal transport, J. Appl. Phys. **93**, 793 (2003).

[2] J.-C. Charlier, X. Blase, and S. Roche, Electronic and transport properties of nanotubes, Rev. Mod. Phys. **79**, 677 (2007).

[3] P. Keblinski, Modeling of heat transport in polymers and their nanocomposites, *Handbook of Materials Modeling* (Springer, Berlin, Heidelberg, 2020), pp. 975–997.

[4] A. Henry, Thermal transport in polymers, Annu. Rev. Heat Transfer **17**, 485 (2014).

[5] D. Mukherji and K. Kremer, Smart polymers for soft materials: From solution processing to organic solids, Polymers **15**, 3229 (2023).

[6] Z. M. Zhang, *Nano/Microscale Heat Transfer*, 2nd ed. (Springer Nature, Switzerland, 2020).

[7] D. Donadio and G. Galli, Atomistic simulations of heat transport in silicon nanowires, Phys. Rev. Lett. **102**, 195901 (2009).

[8] J. Lee, W. Lee, J. Lim, Y. Yu, Q. Kong, J. J. Urban, and P. Yang, Thermal transport in silicon nanowires at high temperature up to 700 K, Nano Lett. **16**, 4133 (2016).

[9] R. S. Prasher, X. J. Hu, Y. Chalopin, N. Mingo, K. Lofgreen, S. Volz, F. Cleri, and P. Keblinski, Turning carbon nanotubes from exceptional heat conductors into insulators, Phys. Rev. Lett. **102**, 105901 (2009).

[10] G. Kim, D. Lee, A. Shanker, L. Shao, M. S. Kwon, Gidley, J. Kim, and K. P. Pipe, High thermal conductivity in amorphous polymer blends by engineered interchain interactions, Nat. Mater. **14**, 295 (2015).

[11] X. Xie, D. Li, T. Tsai, J. Liu, P. V. Braun, and D. G. Cahill, Thermal conductivity, heat capacity, and elastic constants of water-soluble polymers and polymer blends, Macromolecules **49**, 972 (2016).

[12] G. Lv, E. Jensen, C. M. Evans, and D. G. Cahill, High thermal conductivity semicrystalline epoxy resins with anthraquinone-based hardeners, ACS Appl. Polym. Mater. **3**, 4430 (2021).

[13] S. Gottlieb, L. Pigard, Y. K. Ryu, M. Lorenzoni, L. Evangelio, M. Fernández-Regúlez, C. D. Rawlings, M. Spieser, F. Perez-Murano, M. Müller, and A. W. Knoll, Thermal imaging of block copolymers with sub-10 nm resolution, ACS Nano **15**, 9005 (2021).

[14] P.-G. de Gennes, *Scaling Concepts in Polymer Physics* (Cornell University Press, Ithaca, NY, 1979).

[15] M. Doi and S. F. Edwards, *The Theory of Polymer Dynamics* (Oxford Science Publications, UK, 1986).

[16] M. Müller, Process-directed self-assembly of copolymers: Results of and challenges for simulation studies, Prog. Polym. Sci. **101**, 101198 (2020).

[17] D. Mukherji, C. M. Marques, and K. Kremer, Smart responsive polymers: Fundamentals and design principles, Annu. Rev. Condens. Matter Phys. **11**, 271 (2020).

[18] S. Shenogin, A. Bodapati, P. Keblinski, and A. J. H. McGaughey, Predicting the thermal conductivity of inorganic and polymeric glasses: The role of anharmonicity, J. Appl. Phys. **105**, 034906 (2009).

[19] B. Li, F. DeAngelis, G. Chen, and A. Henry, The importance of localized modes spectral contribution to thermal conductivity in amorphous polymers, Commun. Phys. **5**, 323 (2022).

[20] G. R. Desiraju, Hydrogen bridges in crystal engineering: Interactions without borders, Acc. Chem. Res. **35**, 565 (2002).

[21] C. Ruscher, J. Rottler, C. E. Boott, M. J. MacLachlan, and D. Mukherji, Elasticity and thermal transport of commodity plastics, Phys. Rev. Mater. **3**, 125604 (2019).

[22] M. Lim, Z. Rak, J. L. Braun, C. M. Rost, G. N. Kotsonis, P. E. Hopkins, J.-P. Maria, and D. W. Brenner, Influence of mass and charge disorder on the phonon thermal conductivity of entropy stabilized oxides determined by molecular dynamics simulations, J. Appl. Phys. **125**, 055105 (2019).

[23] H. Gao, T. P. W. Menzel, M. H. Müser, and D. Mukherji, Comparing simulated specific heat of liquid polymers and oligomers to experiments, Phys. Rev. Mater. **5**, 065605 (2021).

[24] J. Ahmed, Q. J. Wang, O. Balogun, N. Ren, R. England, and F. Lockwood, Molecular dynamics modeling of thermal conductivity of several hydrocarbon base oils, Tribol. Lett. **71**, 70 (2023).
[25] M. S. Barkhad, B. Abu-Jdayil, A. H. I. Mourad, and M. Z. Iqbal, Thermal insulation and mechanical properties of polylactic acid (PLA) at different processing conditions, Polymers **12**, 2091 (2020).
[26] B. Salameh, S. Yasin, D. A. Fara, and A. M. Zihlif, Dependence of the thermal conductivity of PMMA, PS and PE on temperature and crystallinity, Polymer **45**, 281 (2021).
[27] G. Lv, E. Jensen, C. Shen, K. Yang, C. M. Evans, and D. G. Cahill, Effect of amine hardener molecular structure on the thermal conductivity of epoxy resins, ACS Appl. Polym. Mater. **3**, 259 (2021).
[28] D. Mukherji and M. K. Singh, Tuning thermal transport in highly cross-linked polymers by bond-induced void engineering, Phys. Rev. Mater. **5**, 025602 (2021).
[29] D. Bruns, T. E. de Oliveira, J. Rottler, and D. Mukherji, Tuning morphology and thermal transport of asymmetric smart polymer blends by macromolecular engineering, Macromolecules **52**, 5510 (2019).
[30] R. M. Elder, A. Zaccone, and T. W. Sirk, Identifying nonaffine softening modes in glassy polymer networks: A pathway to chemical design, ACS Macro Letters **8**, 1160 (2019).
[31] F. Demydiuk, M. Solar, H. Meyer, O. Benzerara, W. Paul, and J. Baschnagel, Role of torsional potential in chain conformation, thermodynamics, and glass formation of simulated polybutadiene melts, J. Chem. Phys. **156**, 234902 (2022).
[32] R. Bhowmik, S. Sihn, V. Varshney, A. K. Roy, and J. P. Vernon, Calculation of specific heat of polymers using molecular dynamics simulations, Polymer **167**, 176 (2019).
[33] D. G. Cahill, S. K. Watson, and R. O. Pohl, Lower limit to the thermal conductivity of disordered crystals, Phys. Rev. B **46**, 6131 (1992).
[34] S. Agarwal, N. S. Saxena, and V. Kumar, Temperature dependence thermal conductivity of ZnS/PMMA nanocomposite, in *Physics of Semiconductor Devices. Environmental Science and Engineering*, edited by V. Jain and A. Verma (Springer, Cham, 2014), pp. 737–739.
[35] W. L. Jorgensen, D. S. Maxwell, and J. Tirado-Rives, Development and testing of the OPLS all-atom force field on conformational energetics and properties of organic liquids, J. Am. Chem. Soc. **118**, 11225 (1996).
[36] D. Mukherji, C. M. Marques, T. Stühn, and K. Kremer, Depleted depletion drives polymer swelling in poor solvent mixtures, Nat. Commun. **8**, 1374 (2017).
[37] T. E. de Oliveira, D. Mukherji, K. Kremer, and P. A. Netz, Effects of stereochemistry and copolymerization on the LCST of PNIPAm, J. Chem. Phys. **146**, 034904 (2017).
[38] M. J. Abraham, T. Murtola, R. Schulz, S. Páll, J. C. Smith, B. Hess, and E. Lindahl, GROMACS: High performance molecular simulations through multi-level parallelism from laptops to supercomputers, SoftwareX **1-2**, 19 (2015).
[39] G. Bussi, D. Donadio, and M. Parrinello, Canonical sampling through velocity rescaling, J. Chem. Phys. **126**, 014101 (2007).
[40] H. J. C. Berendsen, J. P. M. Postma, W. F. van Gunsteren, A. DiNola, and J. R. Haak, Molecular dynamics with coupling to an external bath, J. Chem. Phys. **81**, 3684 (1984).
[41] J. Horbach, W. Kob, and K. Binder, Specific heat of amorphous silica within the harmonic approximation, J. Phys. Chem. B **103**, 4104 (1999).
[42] M. H. Müser, Simulation of material properties below the Debye temperature: A path-integral molecular dynamics case study of quartz, J. Chem. Phys. **114**, 6364 (2001).
[43] P. Schöffel and M. H. Müser, Elastic constants of quantum solids by path integral simulations, Phys. Rev. B **63**, 224108 (2001).
[44] T. Feng and X. Ruan, Prediction of spectral phonon mean free path and thermal conductivity with applications to thermoelectrics and thermal management: A review, J. Nanomater. **2014**, 206370 (2014).
[45] E. Lampin, P. L. Palla, P.-A. Francioso, and F. Cleri, Thermal conductivity from approach-to-equilibrium molecular dynamics, J. Appl. Phys. **114**, 033525 (2013).
[46] M. Baggioli and A. Zaccone, Explaining the specific heat of liquids based on instantaneous normal modes, Phys. Rev. E **104**, 014103 (2021).
[47] S. Shen, A. Henry, J. Tong, R. Zheng, and G. Chen, Polyethylene nanofibres with very high thermal conductivities, Nat. Nanotechnol. **5**, 251 (2010).
[48] A. Bhardwaj, A. S. Phani, A. Nojeh, and D. Mukherji, Thermal transport in molecular forests, ACS Nano **15**, 1826 (2021).
[49] T. Zhang and T. Luo, High-contrast, reversible thermal conductivity regulation utilizing the phase transition of polyethylene nanofibers, ACS Nano **7**, 7592 (2013).
[50] H. Ma, Y. Ma, and Z. Tian, Simple theoretical model for thermal conductivity of crystalline polymers, ACS Appl. Polym. Mater. **1**, 2566 (2019).
[51] M. K. Maurya, T. Laschuetza, M. K. Singh, and D. Mukherji, Thermal conductivity of bottle–brush polymers, Langmuir **40**, 4392 (2024).
[52] J. Wu and D. Mukherji, Comparison of all atom and united atom models for thermal transport calculations of amorphous polyethylene, Comput. Mater. Sci. **211**, 111539 (2022).
[53] G. Lv, B. Soman, N. Shan, C. M. Evans, and D. G. Cahill, Effect of linker length and temperature on the thermal conductivity of ethylene dynamic networks, ACS Macro Lett. **10**, 1088 (2021).
[54] M. G. Holland, Phonon scattering in semiconductors from thermal conductivity studies, Phys. Rev. **134**, A471 (1964).
[55] A. V. Savin, Y. A. Kosevich, and A. Cantarero, Semiquantum molecular dynamics simulation of thermal properties and heat transport in low-dimensional nanostructures, Phys. Rev. B **86**, 064305 (2012).
[56] A. V. Savin and Y. S. Kivshar, Modeling of second sound in carbon nanostructures, Phys. Rev. B **105**, 205414 (2022).
[57] M. Pyda, R. Bopp, and B. Wunderlich, Heat capacity of poly(lactic acid), J. Chem. Thermodyn. **36**, 731 (2004).